This article was published in Chemical Engineering Journal, 266, 100-111, 2015
http://dx.doi.org/10.1016/j.cej.2014.12.023

Oxidation of microcystin-LR and cylindrospermopsin by heterogeneous photocatalysis using a tubular photoreactor packed with different TiO_2 coated supports

Lívia X. Pinho [a], Joana Azevedo [b], Sandra M. Miranda [a], Joana Ângelo [c], Adélio Mendes [c], Vítor J.P. Vilar [a,⇑], Vítor Vasconcelos [b,d], Rui A.R. Boaventura [a]

[a] *LSRE – Laboratory of Separation and Reaction Engineering, Associate Laboratory LSRE/LCM, Departamento de Engenharia Química, Faculdade de Engenharia, Universidade do Porto, Rua Dr. Roberto Frias, 4200-465 Porto, Portugal*

[b] *Group of Blue Biotechnology and Ecotoxicology, Interdisciplinary Center of Marine and Environmental Research (CIIMAR/CIMAR), Rua dos Bragas 289, 4050-123 Porto, Portugal*

[c] *LEPABE, Laboratório de Engenharia de Processos, Ambiente, Biotecnologia e Energia, Departamento de Engenharia Química, Faculdade de Engenharia, Universidade do Porto, Rua Dr. Roberto Frias, 4200-465 Porto, Portugal*

[d] *Department of Biology, Faculty of Sciences University of Porto, Rua do Campo Alegre, 4169-007 Porto, Portugal*

Abstract

The photocatalytic degradation of cyanotoxins in aqueous solutions using slurry suspensions of TiO2 implies a post-filtration step to retain the photocatalyst. In this work, 2D and 3D TiO2 thin films sup- ported in inert surfaces was proposed for the solar photocatalytic removal of cyanotoxins microcystin- LR (MC-LR) or cylindrospermopsin (CYN) in distilled and natural water under neutral pH conditions. The photocatalytic experiments were performed in a lab-scale tubular photoreactor with a compound parabolic collector (CPC) using simulated and natural solar radiation. The tubular photoreactor was packed with transparent cellulose acetate monoliths (CAM) coated with a P25 paste or sol–gel 2D TiO2 film or with a photocatalytic 3D TiO2-loaded exterior paint (PC500, VLP7000 and P25). The efficiency of the TiO2 photocatalytic system in the presence of hydrogen peroxide was also assessed. PVC or glass tubes and glass spheres, coated with a photocatalytic 3D TiO2-loaded exterior paint, were also tested as inert surfaces. The supports used in this work were chosen according to some characteristics, such as cost, surface resistance, surface area and transmissibility to UV radiation. The

toxins MC-LR and CYN were purified from *Microcysts aeruginosa* and *Cylindrospermopsis raciborskii* cultures, respectively. The photocatalytic system P25-CAM/H_2O_2 can be considered the most effective process, considering the cyanotoxins removal efficiency, the cost and the simplicity of the preparation.

1. Introduction

Blooms of cyanobacteria have been occurring largely due to the eutrophication of aquatic environments. Many rivers, lakes and reservoirs worldwide develop toxic cyanobacteria. This is especially common during the warmer months where they can appear as greenish suspensions in water. These organisms produce a wide variety of toxins and additional molecules with unknown toxic potential (e.g., microviridins, aeruginosins), and are a challenge for designers of water treatment systems, which depend on the surface raw water quality [1,2]. Although the presence of toxic cyanobacteria/cyanotoxins in water intended for the abstraction of drinking water, agricultural or recreational purposes poses a serious hazard to humans, in which its mechanism of action involves the inhibition of phosphatases directly related to several metabolic functions, this situation has been neglected or at most has been treated on a local level [3].

In recent years, the use of titanium dioxide (TiO_2) as photocatalyst for water treatment has been widely reported, either as a powder in suspension or fixed to various supports [4]. The photo- catalytic reaction involving the irradiation of TiO_2 can only occur using UV light, which corresponds to 4–5% of the solar light spectrum, because of the wide band gap of approximately 3.2 eV of anatase and 3.0 eV of rutile [5–7]. Upon absorption of suitable energy photons, electrons are injected from the valence to the conduction band of the semiconductor creating electron/hole pairs that originate mostly highly oxidizing hydroxyl and highly reduction superoxide radicals [8]. These species lead to the mineralization of different organic pollutants [4,9,10], including cyanotoxins [11]. Photocatalysis using TiO_2 has been previously shown to effectively destroy MC-LR and related toxins in aqueous solutions even at extremely high concentrations [12,13]. Beyond that, the by-products generated during the photocatalytic process appear to be non-toxic [14].

Most studies concerning water treatment using TiO_2 photocatalytic processes apply slurry suspensions of the semiconductor, showing a high degradation and mineralization efficiency of the recalcitrant organic pollutants since the contact of the photocatalyst with the pollutants is promoted with minimal mass transfer limitations and complete/efficient absorption of UV photons that enters in the photoreactor. However, heterogeneous photocatalytic processes are an interesting approach for water decontamination since a post-filtration step to retain the photocatalyst becomes unnecessary, contrary to what happens

when slurry suspensions are used. Since mass transfer is usually the rate-limiting step in these processes applied to liquid phases, the photocatalytic reaction rate can be enhanced by incrementing the catalyst surface [15–18].

Chemical vapor deposition, physical vapor deposition, sputtering and dip-coating are some examples of methods employed to obtain 2D TiO_2 films supported in inert surfaces [19]. Dip coating is a good option because it is simple and the equipment required is not expensive. TiO_2 concentration in the film must be taken into account and adjusted to avoid loss of the catalyst by erosion [20]. Another advantage on the application of immobilized catalyst is the fact that it can be re-used for several treatment cycles while maintaining its stability [18,21].

Mendes and co-workers [17,22,23] developed a coating for immobilizing photocatalysts based on a commercial paint, which is porous (pigment volume concentration slightly above the critical value) and very resistant to photodegradation induced by the presence of the photocatalyst. The pigmentary TiO_2 (rutile) was replaced by the photocatalyst TiO_2 and calcium carbonate (load/ extender). The absence of pigmentary TiO_2 (rutile) allows a greater light penetration, more than 100 1m optical thickness, rending the photocatalytic paint film for photoactive. This 100-1m photoactive porous film is a 3D structure that optimises the light absorbance and has a very high specific active surface area. The main results reported by the same authors showed that the highest yields toward NO photocatalytic oxidation were obtained when incorporating in paint formulations the photocatalysts PC500 (Millennium), PC105 (Millennium), and UV100 (Sachtleben).

The type of material to be used as support is an important factor to be considered, because it directly affects activity, homogeneity, and adhesion of TiO_2 to the surface. Materials like ceramics tiles, paper, glass, fiberglass, and stainless steel have been employed [19,24]. Borosilicate glass or quartz [25], quartz wool [26], glass reactor walls or glass flat plates, raschig rings, glass tubes, glass cylinders [18,27–30], pumice stone [31], monolithic structures (honeycomb) of ceramic [32] or metallic materials [25] have been studied as support. The thin-walled monoliths structures of poly- ethylene terephthalate (PET) and cellulose acetate (CA) are promising alternatives because these are inexpensive, lightweight, easily shaped polymeric materials and UV-transparent [33].

In heterogeneous photocatalysis, the transmittance of the supports and photocatalytic films is crucial to achieve an efficient process, maximizing the illuminated catalyst surface, considering the light path length of the tubular photoreactor. Packing the tubular photoreactor with glass spheres creates shadowed zones, principally in the center of the tube. This “shadowing effect” can be minimized employing a transparent material as support for a thin film catalyst.

Therefore, the purpose of this work was to promote the degradation of *microcystin* (MC-LR) in natural and distilled water solutions at neutral pH values by heterogeneous photocatalysis, using simulated and natural solar UV energy, in a

tubular photoreactor packed with cellulose acetate transparent monoliths (CAM) coated with a P25 paste (made of P25 and Triton^{TM} X-100 as adhesion agent) or sol–gel 2D TiO_2 films and with a photocatalytic 3D TiO_2-loaded exterior paint (PC500, VLP7000 and P25). The efficiency of the TiO_2 photocatalytic system for cyanotoxins degradation was also investigated in the presence of hydrogen peroxide. Other supports, such as PVC or glass tubes and glass spheres were coated with the photocatalytic 3D TiO_2-loaded exterior paint. The best photocatalytic material was further applied in the degradation of *Cylindrospermopsin* (CYN).

2. Experimental

2.1. *Cyanobacteria culture and MC-LR purification*

Stock cultures of cyanobacteria *M. aeruginosa* strain LEGE 91094 (IZANCYA2) and *C. raciborskii* LEGE 97047, were separately inoculated in Z8 medium [34] and kept at 25 ± 1 ºC under fluorescent light (light/dark cycle of 14/10 h), for approximately 30 days. MC- LR was purified from the *M. aeruginosa* culture using the procedure previously described by Raman et al. [35], and CYN from *C. raciborskii* culture, according to the procedure described by Welker et al. [36]. All solvents used in HPLC analyses were high-purity chromatography grade (LiChrosolv, Merck). Aqueous solutions were prepared with Milli-Q ultrapure water supplied from a Millipore water purification system (0.0054 $\mu S\ cm^{-1}$). Reagents used in the culture medium and titanium dioxide (TiO_2) were analytical grade and trifluoroacetic acid (TFA) was 99% spectrophotometric grade. MC-LR used to quantify the MC-LR standard isolated from *M. aeruginosa* (>94% purity, unpublished data) was a reference standard (lot no. MC-LR-a080227, >95% purity), from Cyano Biotech GmbH. Standard CYN was supplied by NCR CRM-Cyn (lot no. 200505310197, 12.6 ppm).

MC-LR solutions were prepared by diluting a concentrate MC- LR stock solution with distilled water. Two different stock solutions were used (Table 1) to eventually detect any difference related to the preparation mode and the influence of the presence of methanol in the MC-LR removal efficiency: (i) 50:50% (v/v) methanol:Milli-Q water equivalent to 0.2% after dilution with distilled water in the lab-scale photoreactor, and (ii) the MC-LR stock solution was further evaporated, allowing preparing a MC-LR solution without the presence of methanol stock solution (100% water); the final pH of both solutions was between 6.5 and 7.0 (without any adjustment). CYN solutions were prepared by diluting a concentrate CYN stock solution with distilled water, resulting in a final pH of around 6.0.

An experiment was carried out using natural water from the Torrão reservoir (Tâmega River, Amarante, Portugal), collected in November 2013. Temperature (T), pH, conductivity and Dissolved Oxygen (DO) were measured *in situ* using a

portable multiparameter analyser (*Hanna Instruments 9828*). Other parameters were determined in laboratory, such as water absorbance at 254 nm, dissolved organic carbon (DOC), total dissolved nitrogen and inorganic ions. Table 2 summarizes the main characteristics of the natural water from the Torrão reservoir. The samples were previously filtered through nylon membrane filters (0.45 1m porosity and 25 mm diameter – Life Sciences). The river water was previously filtered through a GF/C filter from VWR to remove the suspended particles. The UV spectra from MC-LR solution at pH 1.0, 3.0, 7.0 and 12.0, and CYN solution at pH 3.0, 7.0, 9.0 and 12.0, and also from the natural water and natural water spiked with MC-LR or CYN were obtained from a VWR UV-6300 PC Double Beam Spectrophotometer.

2.2. *Catalysts*

Different types of photocatalytic paints and films were prepared with TiO_2 and immobilized in different kinds of inert supports. Briefly, before painted or coated, the supports were soaked for 1 h in distilled water and alkaline detergent (Derquim LM 01, Panreac Química, S.A.U.), then washed exhaustively with Milli-Q water (18.2 MX cm at 25 ºC), and heated up to 50 ºC to dry.

2.2.1. *Paint films formulation*

In the present work, TiO_2 P25 (Degussa), VLP 7000 (Kronos) and PC500 (Millennium) were used to prepare the paint films (Tables 1 and 3). The paint formulation was based on commercial water- based vinyl paint [17] modified by total or partial replacement of the pigmentary TiO_2 by 9 or 12 wt.% of commercial photo-TiO_2 (P25, VLP7000 or PC500), as reported by Águia et al. [22] (Table 1). A glass tube (0.013 m^2), PCV tube – PVCT (0.015 m^2), and glass spheres – GS (1 cm diameter) were painted with TiO_2-based paints in two layers with a brush (Fig. 1). Polyethylene terephthalate transparent monoliths – PETM (type: WaveCore PET150–9/S – width 100 mm, hole diameter 9 mm, thickness tolerance 0.2 mm; Wacosystems), were coated with a thin film of the photocatalytic paint – Pnt(4)-PETM by dip-coating (Dip-Coater RDC21-K, Bungard Elektronik GmbH & Co. KG.). Each layer of the catalyst was depos- ited at a withdrawal rate of 0.8 mm s^{-1}, allowing the formation of a thin and uniform film on the support surface. After depositing each layer, PETM samples were dried at 323 K for 1 h. Finally, the sup- ports were packed into a tubular photocatalytic reactor for the study of MC-LR removal.

2.2.1.1. *2D TiO_2 thin-films.* Cellulose acetate monoliths – CAM (named C: TIMax CA50–9/S – width 80 mm, hole diameter 9 mm, thickness tolerance 0.1 mm; Wacotech GmbH & Co. KG.) were used as support of the catalytic film. 2D TiO_2 thin-films (9 layers) were prepared on CAM samples by combining sol–gel

and dip-coating methods [37], resulting in TiO_2-supported cellulose acetate monoliths (TiO_2-CAM).

2D P25 thin-films (P25-CAM) were prepared on CAM samples according to the method adapted by Quici et al. [38]. P25 in suspension (2% wt.), previously submitted to sonication (10 min under 50 kHz), was used for the deposition of nine layers by dip-coating at a withdrawal rate of 0.8 mm s^{-1}. More details can be seen in Supplementary data file.

2.3. *Photocatalytic films surface characterization*

UV transmittance spectra of uncoated PETM and CAM monoliths, and of samples Pnt(4)-PETM, P25-CAM and TiO_2-CAM with one and two sheets (see Fig. 2), were obtained by using the same spectrophotometer mentioned in Section 2.1.

Scanning electron microscopy (SEM) coupled with energy dispersive X-ray (EDX) analysis was performed at CEMUP using an FEI Quanta 400 FEG ESEM/EDAX Genesis X4 M apparatus equipped with a Schottky field emission gun (for optimal spatial resolution) for the characterization of the surface morphology of, fresh and used (after experiments) Pnt(4)-PETM, Pnt(4)-GS, P25-CAM and TiO_2-CAM, as well as their chemical composition. Each sample was mounted on a double-sided adhesive tape made of carbon for observation at different magnifications; the cross-section of the sample was also measured by this technique.

2.4. *Lab-scale photoreactor*

The oxidation experiments were carried out in a lab-scale photoreactor (Fig. 3) consisting of: (i) a solar radiation simulator (ATLAS, model SUNTEST XLS) with 1100 cm^2 of exposition area, a 1700 W air-cooled xenon arc lamp, a daylight filter and a quartz filter with IR coating; (ii) a compound parabolic collector (CPC) with 0.026 m^2 of illuminated area with anodized aluminum reflectors and borosilicate tube (Schott-Duran type 3.3, Germany, cut-off at 280 nm, internal diameter 46.4 mm, length 161 mm and thickness mm); (iii) one acrylic vessel (capacity of 2.5 L) with a cooling jacket coupled to a thermostatic bath (Lab. Companion, model RW-0525G) to ensure a constant temperature during the experiment; (iv) a magnetic stirrer (Velp Scientifica, model ARE) for complete homogenization of the solution inside the acrylic vessel; (v) one peristaltic pump (Ismatec, model Ecoline VC-380 II, flowrate of 0.65 L min^{-1}) for water recirculation between the CPC and the acrylic vessel; (vi) pH and temperature meter (VWR symphony – SB90M5). Both inlet and outlet polypropylene caps of the tubular photoreactor have four equidistant inlets to ensure a better distribution of the feed solution into the reactor. All the system units were connected using Teflon tube. The intensity of the UV radiation was measured

by a broadband UV radiometer (Kipp & Zonen B.V., model CUV5) placed at the same level than the photoreactor center. The radiometer was connected to a handheld display unit (Kipp & Zonen B.V., model Meteon) to record the incident irradiance (W_{UV} m^{-2}), measured in the wavelength range 280–400 nm. The accumulated UV energy ($Q_{UV,n}$; J L^{-1}) received on any surface, per unit of volume of water inside the reactor, in the time interval Δt was calculated as follows [39]:

$$Q_{UV,n} = Q_{UV,n-1} + \Delta t_n \overline{UV}_{G,n} \frac{A_r}{V_t}; \quad \Delta t_n = t_n - t_{n-1} \qquad (1)$$

where t_n is the time corresponding to n-water sample (s), V_t the total reactor volume (L), A_r the illuminated collector surface area (m^2) and $\overline{UVG}_{,n}$ the average solar ultraviolet incident irradiance (W_{UV} m^{-2}) measured during the period Δt_n (s).

2.5. *Experimental setup*

The borosilicate tube of the photoreactor was packed with different TiO_2 – coated supports: (i) TiO_2-based paints (deposited on PVCT, glass tube, GS or PETM); (ii) TiO_2 thin-films (sol–gel TiO_2 or P25 deposited on CAM). Prior to the experiments using TiO_2-paints, the photocatalytic paint was activated under solar UV radiation by recirculating water without toxin for 7–8 h. Afterwards the system was washed with distilled water before use.

The recirculation acrylic vessel was filled with 2.4 L of MC-LR solution (~100 μg L^{-1}) or CYN solution (~70 μg L^{-1}) and homogenized by stirring during 15 min in the darkness and a control sample was taken. The temperature set-point of the refrigerated thermostatic bath was set at 25 ºC. Afterwards, the water was pumped to the CPC unit and recirculated in the closed system during 40 min in the darkness and a new sample was taken to observe if any adsorption occurred. After that, the SUNTEST was turned on and the irradiance was set at 500 W m^{-2}, which is equivalent to 44 W_{UV} m^{-2}. When necessary, an initial H_2O_2 concentration of 25 mg L^{-1} was added. Samples were taken at pre-defined times to evaluate the removal progress and analysis was done in duplicate.

2.6. *Analytical procedures*

Solid-phase extraction (SPE) was used to concentrate toxins and clean-up the sample before MC-LR detection with the aid of a Vacuum Manifold VWR and a

vacuum pump ILMVAC, and a Strata C18-E (55 um, 70 A) 500 mg/6 mL cartridge. The analytical procedures on MC-LR, CYN, H_2O_2, dissolved organic carbon (DOC), dis- solved nitrogen and inorganic ions concentration measurement are reported in the Supplementary data file.

3. Results and discussion

3.1. *Photocatalytic films surface characterization*

The "shadowing effect" can be minimized employing transparent monoliths as a support for the thin film catalyst, as for example PET or CAM monoliths. Fig. 2 shows the transmittance spectra for PET and CAM monoliths with or without coating, and considering one or two sheets. Although CAM monoliths present a higher transmissibility than PET ones, both materials show more than 80% transmissibility for wavelengths between 300–800 nm, indicating that these supports can be used for solar photocatalytic applications. The high transmissibility is also observed when the light has to cross two sheets of the monoliths, considering the path length in the tubular photoreactor.

On the other hand, it can be observed a significant transmittance reduction for the coated monoliths when compared to the uncoated monoliths, especially in the case of Pnt(4)-PETM, revealing the presence of an opaque film. Águia et al. [22] reported that the transmittance of a paint formulation similar to those used in this work, is negligible. However, transmittance spectra for P25- CAM and TiO_2-CAM samples show a significant increment of transmissibility mainly for wavelengths higher than 350 nm, considering the first outermost sheet (outside the hole). The transmissibility decreased considerably for the second sheet after empty space and is even lower in the middle (after going through the two sheets) (Fig. 1d). It is worth mentioning the amount of TiO_2 deposited on each monolith: 0.0946 g for P25-CAM and 0.1632 g for TiO_2-CAM.

The surface morphology and chemical composition of the films Pnt(4)-PETM, Pnt(4)-GS, P25-CAM and TiO_2-CAM, before (fresh films) and after the photocatalytic process, was determined by SEM/EDX (Figs. 4 and 5).

All the EDX determinations showed a high amount of carbon, which can be related to the adhesive tape made of carbon, where each sample was mounted before observation (see Section 2.4). The glass spheres painted by hand with Pnt(4) (Pnt(4)-GS) present a substantially thicker layer (144–159 μm) (Fig. 4a–c) than PETM coated by dip-coating (34–37 μm) (Fig. 4d–f). The PETM films seem to be more uniform and homogeneous than painted glass spheres (Fig. 4a and d). Fig. 4e and f show that the film thickness of the photocatalytic paint before the experiment is much higher than after the experiment. This can be mainly associated to the heterogeneous film thickness along the walls of the monoliths, since the images were obtained from different parts of the monoliths.

According to the EDX spectra, the proportion of each element remained

approximately the same after the photocatalytic experiments using the Pnt(4)-PETM samples (Fig. 4g and h). Similar results were reported by Monteiro et al. [40] using a photocatalytic paint (four layers of photocatalytic paint in CAM; 9 wt.% of photo- TiO_2) for perchloroethylene removal at gas phase.

The film thickness was also determined from the cross-section images obtained for TiO_2-CAM (Fig. 5b) and P25-CAM (Fig. 5e). The TiO_2-CAM film thickness (always between 420 and 436 nm) was relatively uniform along the whole surface of the monolith. The layers thickness for the monoliths prepared with P25 is less uniform, varying from 0.867 to 1.118 μm. The P25-CAM and TiO_2-CAM films thickness remained almost similar before and after the photo-catalytic process, even taken into account that the images were obtained at different parts of the monolith structure. The surface of P25-CAM has the same appearance of the film obtained by Sampaio et al. [41] in nanotubes coated with TiO_2 film, consisting of a granular texture due to the spheroidal shape of the TiO_2 particles.

Fig. 5d shows that the P25-CAM film structure is mainly composed of agglomerated particles, superimposed on top of each other (Fig. 5d), while the TiO_2-CAM film has a more uniform surface (Fig. 5a) probably due to the lower size of the TiO_2 particles. Several cracking fissures can be observed in the TiO_2-CAM film, producing a mosaic of flake-like forms, probably due to the thermal expansion coefficients of the CAM material and the TiO_2 [42] produced by the sol–gel procedure (dry step); or, less probable, the fissures could be generated during the SEM analysis due to the high energy of the incident irradiation.

Film delamination also occurs after the photocatalytic experiments (data not shown), where many fissures are brighter probably also due to the SEM light scattering promoted by delaminated film or, less probably, due to the partial filling of such fissures with some organics [43]. Lopes et al. [43] tested the same material for gas phase for perchloroethylene degradation, and observed the same appearance after the photocatalytic process; however, a high photocatalytic activity was still obtained after the observed delamination of the film. Regardless of the fissures in the surface of TiO_2-CAM, our previous reports confirmed their stability and resistance for more than 50 h in perchloroethylene elimination [43].

The EDX spectra showed that the proportion of each element remained approximately constant for both samples, before (Fig. 5g and h) and after the photocatalytic process (data not shown).

3.2. *Oxidation of MC-LR by photocatalysis using TiO_2 based paint*

This section evaluates the photocatalytic efficiency of TiO_2 based paints using different types of TiO_2 and immobilized in different support (Table 1). Experiments were carried out without catalyst: (i) photolysis (water/MC-LR/UV) and (ii) photolysis-paint (water/MC-LR/PVC tube painted with based

paint/UV). MC-LR oxidation was negligible in both situations, i.e. more than 88 and 85% of MC-LR was detected, respectively, after an accumulated UV energy of 10 kJ L^{-1} (6 h) (Fig. 6), which is in agreement with the almost negligible absorption of solar UV–visible radiation by the MC-LR molecule (Fig. 7b). In fact, several authors reported that MC-LR removal by UV radiation alone is not efficient [9,11,44– 47], since the cyclic structure of the MC-LR (Fig. 7c) provides a high stability under sunlight and high temperatures (they can with- stand after many hours of boiling) [48–51].

Because the purified solution of MC-LR contains MeOH as solvent, its influence in the degradation of MC-LR was studied. The results are shown in Fig. 8a for sample Pnt(4)-PVCT(M) which is compared with sample Pnt(4)-PVCT(W), without methanol. The presence of methanol inhibited the photocatalytic process efficiency in less than 10%, acting as a scavenger of hydroxyl radicals. Dark experiments performed with all TiO_2-based paints showed 0–10% toxin adsorption under the operational conditions of pH between 6.5 and 7.0 (Fig. 8a and b). MC-LR contains two ionisable carboxyl groups and one ionisable amino group that are not part of peptide bonds that make up the cyclic peptide structure [52] (Fig. 7c). The pK_a values of the carboxyl groups have been reported to be 2.17 and 3.96 [53]. The intermediate species ($H_2MC^{\pm}$) is a zwitterion due to the protonated amine moiety associated with the arginine group of MC-LR (Fig. 7a). De Maggd et al. [54] showed that the dissociation of this amine group likely occurs at pH > 9. For pH values higher than the point of zero charge of TiO_2 (PZC = 6.7) [55], its surface becomes hydroxylated ($TiOH^-$) and the overall surface becomes negatively charged. The MC-LR molecule is also negatively charged for pH values higher than 6.0, explaining the low adsorption on the TiO_2 surface, since all the experiments were per- formed at pH values between 6.5 and 7.0. Pelaez et al. [56] using films of NF-TiO_2, during 5 h of experiments in dark, concluded that the adsorption of MC-LR (initial MC-LR concentration of 500 $\mu g\ L^{-1}$) was approximately 39.6% at pH 3.0, 30.1% at pH 5.7, 9.2% at pH 7.1 and 7.9% at pH 8.0, which is well correlated with the charge of MC-LR molecules and TiO_2 surface according to the solution pH.

Fig. 8a shows that the photocatalytic process using the Pnt(1), Pnt(2) and Pnt(3) TiO_2-based paints presents low MC-LR removal efficiencies (10–17%). Further experiments with photocatalytic paints were performed by increasing the photoactive TiO_2 concentration (PC500) and changing the inert support. PC500 was chosen as the photocatalyst since Águia et al. [17] reported a higher efficiency in the photo-oxidation of NO, using total replacement of the pigmentary TiO_2; moreover its activation step does not have to be harsher when compared to P25.

Pnt(4)-PVCT-M presents a higher efficiency in MC-LR removal (39%) when compared with Pnt(1), Pnt(2) and Pnt(3) (Table 1), which can be associated to the higher TiO_2 concentration (12%/0.25g; 100 mg L^{-1}) achieved by the total

replacement of the pigmentary TiO_2 and higher light penetration. Moreover, in the Pnt(4)-PVCT-M the paint was deposited on a PVC tube with a larger diameter, which is comparable to the glass tube: not prone to ageing, practical, low cost (as glass) and is also an inert material, which does not increase the DOC of the solution.

Two others experiments were performed using the formulation Pnt(4) with 12 wt.% of TiO_2 and total pigmentary TiO_2 replacement, supported in glass spheres (Pnt(4)-GS) and PET (Pnt(4)-PETM).

Despite the formulation of Pnt(4)-GS presented the highest TiO_2 concentration (600 mg L^{-1}), it did not lead to the best result. Probably, when the tubular photoreactor is packed with glass spheres, only a small part of the catalyst surface area is exposed to UV light, due to "shading effect", mainly for the spheres that are in the center of the tube. Beyond that, the glass spheres were painted by hand, resulting in a ticker layer (±150 μm), and probably a fraction of the TiO_2 particles were not being illuminated.

The use of transparent PET monoliths coated with Pnt(4), led to a substantial increase on MC-LR removal efficiency, more than 7 times than using the glass or PVC cylindrical tube, mainly attributed to the higher UV transmissibility of the support and efficient use of the UV photons. A significant adsorption of MC-LR in TiO_2 based paints was also observed (25%) for the Pnt(4)-PETM system, probably associated with the higher TiO_2 concentration and surface area.

3.3. *Oxidation of MC-LR by photocatalysis using TiO_2 based paint and H_2O_2*

Experiments with the addition of H_2O_2 were also carried out using Pnt(4) formulation: Pnt(4)-PVCT-W/H_2O_2 and Pnt(4)-PETM/ H_2O_2 (Fig. 8b). The addition of H_2O_2 (initial concentration of 25 mg L^{-1}) showed a positive effect on the prevention of the electron–hole recombination by accepting photogenerated electrons from the conduction band (Eq. (2)) and in the production of additional OH radicals through reactions (2) and (3) [57].

$$H_2O_2 + e^-_{CB} \rightarrow OH^{\cdot} + OH^- \quad (2)$$

$$H_2O_2 + O_2^{\cdot -} \rightarrow OH^{\cdot} + OH^- + O_2 \quad (3)$$

The kinetic profiles show a very fast initial reaction rate until 2 kJ_{UV} L^{-1}, followed by a slow process, which can be attributed to the competition of hydroxyl radicals for the initial intermediates generated and the MC-LR molecules.

The addition of H_2O_2 to Pnt(4) using the cylindrical PVC tube as support for the photocatalytic paint (Pnt(4)-PVCT-W/H_2O_2), led to an increment in the removal by 31%, when compared with Pnt(4)- PVCT-W system, achieving a final MC-LR removal efficiency of almost 70% after 10 kJ_{UV} L^{-1} and consuming 13 mM of

H_2O_2. On the other hand, the Pnt(4)-PETM/H_2O_2 system achieved a MC-LR removal of 93% after 11 kJ$_{UV}$ L^{-1} and consuming only 2 mM of H_2O_2, which corresponds to an increment in the photocatalytic efficiency of 28% when compared with the Pnt(4)-PETM system.

MC-LR removal is negligible using the H_2O_2/UV–visible system (Fig. 6), mainly due to the low oxidation potential of H_2O_2. Moreover, a negligible fraction of UVA–visible solar radiation is absorbed by the MC-LR molecule (Fig. 7b) and photolysis of H_2O_2 is not significant due to the fact that radiation below 280 nm is needed for an effective H_2O_2 cleavage (the borosilicate glass tube has a cut-off at 280 nm).

3.4. *Oxidation of MC-LR by photocatalysis using TiO2 thin films*

In the experiments using TiO_2 thin films (P25-CAM and TiO_2- CAM), a 19% decrease in MC-LR concentration was observed in the dark experiments, attributed to the adsorption of MC-LR on the catalyst surface (Fig. 9a), just as happened in the system Pnt(4)-PETM, probably because of the higher TiO_2 concentration and surface area.

MC-LR removal by TiO_2-CAM and P25-CAM achieved 97% and 90% efficiency after 5 kJ L^{-1}, respectively (Fig. 9a). The photocatalytic degradation process follows pseudo-first-order kinetics with $k = 0.32 \pm 0.03$ L kJ^{-1} and $k = 0.49 \pm 0.03$ L kJ^{-1}, respectively for P25-CAM and TiO_2-CAM systems. The slightly higher efficiency of TiO_2-CAM when compared with P25-CAM can be mainly attributed to the higher concentration of TiO_2 deposited on the surface of the CAM structure.

The higher efficiency of the P25 paste or sol–gel TiO_2 films when compared with the TiO_2-loaded exterior paints can be mainly associated with the mass transfer limitations inside the porous structure of the paint, and also to the poor efficient absorption of UV photons by the catalytic paint-bed. Antoniou et al. [48] used a TiO_2–sol–gel thin film after three dip-coatings-calcinations on glass substrate to destroy MC-LR by photocatalysis, achieving ~50% MC-LR removal (C_O ~ 2000 μg L^{-1}; pH ~ 6.8) after 4 h. At acidic pH (3.0) the photocatalytic efficiency increased substantially to values higher than 85% mainly associated with attractive forces between the positively charged titania ($TiOH^+$) and negatively charged toxin ($H_2MC^{\pm}$ and HMC^-). Although low pH favors substantially the photocatalytic process efficiency, in a full-scale treatment plant, costs associated with the acidification/neutralization steps may be high and the addition of high amounts of sodium hydroxide (NaOH) or chloride acid (HCl) to water for human consumption is not possible. Feng et al. [58] studied the photocatalytic removal of MC-LR (C_0 = 20 μg L^{-1}) using a nano-TiO_2 thin film, prepared by sol–gel and dip-coating methods, and a UV 365 nm lamp, obtaining over 95% removal after 120

min at pH 4.0. Liu et al. [59] used a carbon-based surfactant-assisted sol–gel method to synthesize visible-light-active C–N–TiO_2 immobilized on a borosilicate glass, to destroy MC-LR (C_0 = 500 $\mu g\ L^{-1}$ and pH 3), under visible light irradiation provided by two 15 W fluorescent lamps, and obtained between 70% and 80% removal for all films tested, after 5 h exposure.

3.5. *Oxidation of MC-LR by photocatalysis using TiO2 thin films with natural solar light*

In the present work P25-CAM proved to be the best thin film formulation, because it allows a simpler and cheaper process, and the results obtained are similar to the ones obtained by TiO_2-CAM, although with a lower TiO_2 concentration. For all these reasons, P25-CAM was chosen for the photocatalytic tests with natural solar light or addition of H_2O_2.

The photocatalytic reaction using P25-CAM under natural UV radiation ($\bar{T}$ =27 °C; $\bar{U}V$ = 38 W m^{-2}) shows a similar MC-LR removal when compared to that obtained using simulated solar radiation with a constant UV irradiance of 44 W$_{UV}$ m^{-2} (Fig. 9b).

3.6. *Oxidation of MC-LR by photocatalysis using TiO2 thin films and H2O2*

The addition of H_2O_2 to the P25-CAM system under simulated solar light, increased substantially the initial photocatalytic reaction rate, being necessary only 1.26 mM of H_2O_2 to achieve 85% MC-LR removal after 1 kJ L^{-1} accumulated energy, compared to only 20% of MC-LR removal after the same reaction period without H_2O_2 addition. Comparing the pseudo-first-order kinetic parameters (Table S1) one can conclude that the best system is P25-CAM/H_2O_2 ($k = 2.0 \pm 0.4$ L kJ^{-1} and $r_0 = (18 \pm 4)$ x 10 $\mu g\ kJ^{-1}$). The reaction rate decreases along the reaction, which can be attributed to the competition of hydroxyl radicals between the initial inter- mediates generated and the MC-LR molecules.

A final photocatalytic experiment using natural water from the Torrão reservoir (Tâmega River, Portugal) spiked with ~ 100 $\mu g\ L^{-1}$ MC-LR (P25-CAM-n.w) was performed, in order to evaluate the influence of other inorganic and organic species present in surface waters in MC-LR removal. The characteristics of the natural water are given in Table 2. Fig. 9b shows a slow MC-LR degradation kinetic profile principally in the initial part of the reaction, when compared with the experiments performed with distilled water, being necessary an amount of UV energy more than 10 times higher for the system with river water and 2.75 mM of H_2O_2 to achieve 90% MC-LR removal. Although the amount of dissolved organic carbon present in the natural water is low (2.2 mg C L^{-1}), which is mainly attributed

to the presence of recalcitrant humic substances, its concentration is several times higher than the contribution of MC-LR for DOC. Those recalcitrant organic substances can compete for the UV photons and hydroxyls radicals as well as they can act as photosensitizers [60].

3.7. *Oxidation of CYN by photocatalysis using TiO2 thin film*

Some experiments were carried out to assess the CYN removal efficiency using one of the materials that showed good results with respect to MC-LR removal (P25-CAM and P25-CAM/H_2O_2). The initial CYN concentration was around 70 $\mu g\ L^{-1}$, a typical concentration found in water reservoirs [61,62].

CYN is very stable, as it was proven by Chiswell et al. [62] in a work where they studied the effect of temperature and pH on the decomposition of CYN in darkness. The authors boiled an aqueous extract of *C. raciborskii* containing 2.5 mg L^{-1} of CYN for 15 min and no effect on the concentration was observed. Experiments were also performed at pH 4, 7 and 10. After 8 weeks at room tempera- ture of 22 ºC, CYN maintained 75% of the initial concentration (4 mg L^{-1}).

A negligible fraction of UVA-Vis solar radiation is absorbed by the CYN molecule at different pH values (spectra not showed), which reflects the negligible effect of photolysis in CYN concentration (see Fig. S1a). No photolysis was also observed by He and collaborators [63] when using a 254 nm UV lamp to degrade CYN. Beyond that, after a period of 40 min in dark, no significant adsorption of CYN in TiO_2 thin film was detected. Similarly, Senogles et al. [61] showed negligible adsorption of CYN in the dark, using 0.1 g L^{-1} TiO_2, at pH = 4, pH = 7 and pH = 9. With a reported pK_a value of 8.8, CYN is mainly present as a zwitterion, with an overall zero charge at pH ≤ 7.4 [63,64], due to the negatively charged sulfate group and the positively charged guanidine group [65]. The marginal adsorption observed in these experiments (Fig. 10) can thus be explained by the fact that at pH = 6, CYN molecules and TiO_2 particles are neutral species, so negligible attraction between them occurs.

No difference was observed when using P25-CAM-CYN with simulated and natural solar UV radiation as regards CYN removal: 47% after Q_{UV} ~ 9 kJ L^{-1} in both cases (Fig. 10a). The addition of H_2O_2 (P25-CAM-CYN/H_2O_2/UV) (Fig. 10b) showed a negligible effect on the reaction rate, leading to only 40% removal, a value comparable to that obtained without H_2O_2 addition and the same energy (~9 kJ_{UV} L^{-1}), and after 15.6 kJ_{UV} L^{-1} the removal raised to 55%. The result from the H_2O_2/UV experiment was similar to that obtained by photolysis (Fig 10b): ~10% removal after 10 kJ_{UV} L^{-1} accumulated energy.

To investigate the influence of the natural organic material in CYN removal, an experiment was carried out with river water (P25-CAM-CYN/H_2O_2/river water,

Fig. 10b) from the same source of the natural water used in the MC-LR experiment (Table 2). In this experiment 85% CYN removal was achieved after ~16 kJUV L^{-1} with $r_0 = 14 \pm 0.9$ μg kJ^{-1}, whereas when distilled water was used (P25-CAM-CYN/H_2O_2) r_0 was only 6 ± 1 μg kJ^{-1}. Senogles et al. [61] achieved a similar result in the degradation of CYN spiked (90 μg L^{-1}) in raw water from North Pine Dam using a photocatalytic process with P25 in slurry conditions, achieving a CYN half- life of 4.4 min, against 16.1 min using Milli-Q water; the authors indicated that the presence of other organic and inorganic matter in the natural water can potentially enhance the photocatalytic reaction.

4. Conclusions

CAM or PET monoliths are a good supports for photocatalysts, when compared with cylindrical glass or PVC tubes and glass spheres. They present honeycomb three-dimensional transparent arrays, large specific photoactive surface area and consequently increased light absorption, rugged surface that enables good adhesion of the catalytic coatings.

The photocatalytic oxidation of MC-LR at neutral pH values was achieved successfully using different heterogeneous solar photo- catalytic processes, avoiding the need of acidification/neutralization steps, as well as the post-filtration step required when slurry suspensions of the photocatalyst are used. The higher efficiency of P25 paste and sol–gel 2D TiO_2 films deposited in CAM when compared with 3D TiO_2-loaded exterior paints can be mainly associated with mass transfer limitations inside the porous structure of the paint and with the poor efficient absorption of UV pho- tons by the catalytic paint-bed.

The addition of H_2O_2 to the P25-CAM system enhanced substantially the MC-LR removal rate, whereby less than 1 kJUV L^{-1} accumulated energy was required to achieve more than 85% MC-LR removal (C_0 ~ 100 μg L^{-1}). The presence of H_2O_2 also enhanced significantly the efficiency of the photocatalytic paints associated with the production of additional OH radicals. As regards CYN removal, although TiO_2 photocatalysis seems to be a good process, a long exposure time is required. Although the presence of organic and inorganic matter in river water impairs significantly the MC-LR removal rate, the degradation rate of CYN was enhanced significantly. The proposed heterogeneous photocatalytic system driven by solar energy can be an interesting technology to be implemented in remote areas not reached by the drinking water network, with a high availability of solar radiation, for the removal of cyanotoxins present in natural waters.

Acknowledgements

This work was co-financed by FCT and FEDER under Programme COMPETE (Projects PEst-C/EQB/LA0020/2013 and PesT-C/MAR/ LA0015/2013) as also by

QREN, ON2 and FEDER through project NORTE-07-0162-FEDER-000050. Lívia X. Pinho acknowledges her PhD scholarship from CNPQ-Brasil (200544/2010-1). V.J.P. Vilar acknowledges the FCT Investigator 2013 Programme (IF/01501/ 2013).

Appendix A. Supplementary data

Supplementary data associated with this article can be found, in the online version, at http://dx.doi.org/10.1016/j.cej.2014.12.023.

References

1. I.R. Falconer, A.R. Humpage, Health risk assessment of *Cyanobacterial* (blue- green algal) toxins in drinking water, Int. J. Environ. Res. Publ. Health 2 (2005) 43–50.
2. S.J. Hoeger, B.C. Hitzfeld, D.R. Dietrich, Occurrence and elimination of cyanobacterial toxins in drinking water treatment plants, Toxicol. Appl. Pharmacol. 203 (2005) 231–242.
3. B. Hitzfeld, S. Höger, D. Dietrich, Cyanobacterial toxins: removal during drinking water treatment, and human risk assessment, Environ. Health Perspect. 108 (2000) 113.
4. D. Robert, S. Malato, Solar photocatalysis: a clean process for water detoxification, Sci. Total Environ. 291 (2002) 85–97.
5. C. Han, M. Pelaez, V. Likodimos, A.G. Kontos, P. Falaras, K. O'shea, D.D. Dionysiou, Innovative visible light-activated sulfur doped TiO2 films for water treatment, Appl. Catal., B 107 (2011) 77–87.
6. M. Pelaez, A.A. De La Cruz, E. Stathatos, P. Falaras, D.D. Dionysiou, Visible light- activated N-F-codoped TiO2 nanoparticles for the photocatalytic degradation of microcystin-LR in water, Catal. Today 144 (2009) 19–25.
7. X. Yang, C. Cao, L. Erickson, K. Hohn, R. Maghirang, K. Klabunde, Photo-catalytic degradation of rhodamine B on C-, S-, N-, and Fe-doped TiO2 under visible-light irradiation, Appl. Catal., B 91 (2009) 657–662.
8. I.O. Masao Kaneko, Photocatalysis Science and Technology, Kodansha, Springer, Tokyo, 2002, pp. 9–28.
9. T.M. Triantis, T. Fotiou, T. Kaloudis, A.G. Kontos, P. Falaras, D.D. Dionysiou, M. Pelaez, A. Hiskia, Photocatalytic degradation and mineralization of microcystin-LR under UV-A, solar and visible light using nanostructured nitrogen doped TiO2, J. Hazard. Mater. 211–212 (2012) 196–202.
10. J.M.C. Robertson, P.K.J. Robertson, L.A. Lawton, A comparison of the effectiveness of TiO2 photocatalysis and UVA photolysis for the destruction of three pathogenic micro-organisms, J. Photochem. Photobiol. A: Chem. 175 (2005) 51–56.
11. L.X. Pinho, J. Azevedo, V.M. Vasconcelos, V.J.P. Vilar, R.A.R.

Boaventura, Decomposition of *Microcystis aeruginosa* and microcystin-LR by TiO2 oxidation using artificial UV light or natural sunlight, J. Adv. Oxidation Technol. 15 (2012) 98–106.
12. M.G. Antoniou, A. Armah, D.D. Dionysiou, Cyanotoxins: new generation of water contaminants, J. Environ. Eng. 131 (2005) 1239.
13. Liu, L.A. Lawton, D.W. Bahnemann, L. Liu, B. Proft, P.K.J. Robertson, The photocatalytic decomposition of microcystin-LR using selected titanium dioxide materials, Chemosphere 76 (2009) 549–553.
14. I. Liu, L.A. Lawton, B. Cornish, P.K.J. Robertson, Mechanistic and toxicity studies of the photocatalytic oxidation of microcystin-LR, J. Photochem. Photobiol. A: Chem. 148 (2002) 349–354.
15. D. Gumy, A.G. Rincon, R. Hajdu, C. Pulgarin, Solar photocatalysis for detoxification and disinfection of water: different types of suspended and fixed TiO2 catalysts study, Solar Energy 80 (2006) 1376–1381.
16. D. Robert, A. Piscopo, O. Heintz, J.V. Weber, Photocatalytic detoxification with TiO2 supported on glass-fibre by using artificial and natural light, Catal. Today 54 (1999) 291–296.
17. C. Águia, J. Ângelo, L.M. Madeira, A. Mendes, Photo-oxidation of NO using an exterior paint – screening of various commercial titania in powder pressed and paint films, J. Environ. Manage. 92 (2011) 1724–1732.
18. R. Van Grieken, J. Marugán, C. Sordo, C. Pablos, Comparison of the photocatalytic disinfection of *E. coli* suspensions in slurry, wall and fixed-bed reactors, Catal. Today 144 (2009) 48–54.
19. A.I. Cardona, R. Candal, B. Sánchez, P. Ávila, M. Rebollar, TiO2 on magnesium silicate monolith: effects of different preparation techniques on the photocatalytic oxidation of chlorinated hydrocarbons, Energy 29 (2004) 845–852.
20. P. Ávila, B. Sánchez, A.I. Cardona, M. Rebollar, R. Candal, Influence of the methods of TiO2 incorporation in monolithic catalysts for the photocatalytic destruction of chlorinated hydrocarbons in gas phase, Catal. Today 76 (2002) 271–278.
21. A.C. Garcia, S. Bargu, P. Dash, N.N. Rabalais, M. Sutor, W. Morrison, N.D. Walker, Evaluating the potential risk of microcystins to blue crab (*Callinectes sapidus*) fisheries and human health in a eutrophic estuary, Harmful Algae 9 (2010) 134–143.
22. C. Águia, J. Ângelo, L.M. Madeira, A. Mendes, Influence of photocatalytic paint components on the photoactivity of P25 towards NO abatement, Catal. Today 151 (2010) 77–83.
23. C. Águia, J. Ângelo, L.M. Madeira, A. Mendes, Influence of paint components on photoactivity of P25 titania toward NO abatement, Polym. Degrad. Stab. 96 (2011) 898–906.
24. G.S. Shephard, S. Stockenström, D. De Villiers, W.J. Engelbrecht, G.F.S. Wessels, Degradation of microcystin toxins in a falling film photocatalytic

reactor with immobilized titanium dioxide catalyst, Water Res. 36 (2002) 140–146.
25. H. Choi, E. Stathatos, D.D. Dionysiou, Sol–gel preparation of mesoporous photocatalytic TiO2 films and TiO2/Al2O3 composite membranes for environmental applications, Appl. Catal., B 63 (2006) 60–67.
26. G. Vella, G.E. Imoberdorf, A. Sclafani, A.E. Cassano, O.M. Alfano, L. Rizzuti, Modeling of a TiO2-coated quartz wool packed bed photocatalytic reactor, Appl. Catal., B 96 (2010) 399–407.
27. M.D. Hernández-Alonso, I. Tejedor-Tejedor, J.M. Coronado, J. Soria, M.A. Anderson, Sol–gel preparation of TiO2–ZrO2 thin films supported on glass rings: Influence of phase composition on photocatalytic activity, Thin Solid Films 502 (2006) 125–131.
28. C. Sordo, R. Van Grieken, J. Marugán, P. Fernández-Ibáñez, Solar Photocatalytic Disinfection with Immobilised TiO2 at Pilot-plant Scale, in 2010, pp. 507– 512.
29. C. Pablos, R. Van Grieken, J. Marugań , A. Muñoz, Simultaneous photocatalytic oxidation of pharmaceuticals and inactivation of *Escherichia coli* in wastewater treatment plant effluents with suspended and immobilised TiO2, Water Sci. Technol. 65 (2012) 2016–2023.
30. R. Van Grieken, J. Marugán, C. Sordo, P. Martínez, C. Pablos, Photocatalytic inactivation of bacteria in water using suspended and immobilized silver-TiO2, Appl. Catal., B 93 (2009) 112–118.
31. M. Subrahmanyam, P. Boule, V. Durga Kumari, D. Naveen Kumar, M. Sancelme, Rachel, Pumice stone supported titanium dioxide for removal of pathogen in drinking water and recalcitrant in wastewater, Solar Energy 82 (2008) 1099– 1106.
32. P. Avila, A. Bahamonde, J. Blanco, B. Sánchez, A.I. Cardona, M. Romero, Gas- phase photo-assisted mineralization of volatile organic compounds by monolithic titania catalysts, Appl. Catal., B 17 (1998) 75–88.
33. R. Portela, B. Sánchez, J.M. Coronado, R. Candal, S. Suárez, Selection of TiO2- support: UV-transparent alternatives and long-term use limitations for H2S removal, Catal. Today 129 (2007) 223–230.
34. J. Kotai, Instructions for preparation of modified nutrient solution Z8 for algae, Norw. Inst. Water Res. 11 (1972) 5.
35. S. Ramanan, J. Tang, A. Velayudhan, Isolation and preparative purification of microcystin variants, J. Chromatogr. A 883 (2000) 103–112.
36. M. Welker, H. Bickel, J. Fastner, HPLC-PDA detection of cylindrospermopsin– opportunities and limits, Water Res. 36 (2002) 4659–4663.
37. M.A. Anderson, L.W. Miller, Tejedor-Anderson, M. Isabel, A waveguide comprising a transparent substrate and a metal oxide coating having the disclosed properties on the substrate can propagate light in an

attenuated total reflection mode, in: United States Patent 2001.
38. N. Quici, M.L. Vera, H. Choi, G.L. Puma, D.D. Dionysiou, M.I. Litter, H. Destaillats, Effect of key parameters on the photocatalytic oxidation of toluene at low concentrations in air under 254 nm UV irradiation, Appl. Catal., B 95 (2010) 312–319.
39. S. Malato, J. Blanco, A. Vidal, C. Richter, Photocatalysis with solar energy at a pilot-plant scale: an overview, Appl. Catal., B 37 (2002) 1–15.
40. R.A.R. Monteiro, F.V.S. Lopes, A.M.T. Silva, J. Ângelo, G.V. Silva, A.M. Mendes, R.A.R. Boaventura, V.J.P. Vilar, Are TiO2-based exterior paints useful catalysts for gas-phase photooxidation processes? a case study on n-decane abatement for air detoxification, Appl. Catal., B 147 (2014) 988–999.
41. M.J. Sampaio, C.G. Silva, A.M.T. Silva, V.J.P. Vilar, R.A.R. Boaventura, J.L. Faria, Photocatalytic activity of TiO2-coated glass raschig rings on the degradation of phenolic derivatives under simulated solar light irradiation, Chem. Eng. J. 224 (2013) 32–38.
42. K. Narasimha Rao, Studies on thin film materials on acrylics for optical applications, Bull. Mater. Sci. 26 (2003) 239–245.
43. F.V.S. Lopes, S.M. Miranda, R.A.R. Monteiro, S.D.S. Martins, A.M.T. Silva, J.L. Faria, R.A.R. Boaventura, V.J.P. Vilar, Perchloroethylene gas-phase degradation over titania-coated transparent monoliths, Appl. Catal., B 140–141 (2013) 444–456.
44. A. Feitz, T. Waite, G. Jones, B. Boyden, P. Orr, Photocatalytic degradation of the blue green algal toxin microcystin-LR in a natural organic-aqueous matrix, Environ. Sci. Technol. 33 (1999) 243–249.
45. L. Lawton, P. Robertson, B. Cornish, I. Marr, M. Jaspars, Processes influencing surface interaction and photocatalytic destruction of microcystins on titanium dioxide photocatalysts, J. Catal. 213 (2003) 109–113.
46. P. Robertson, L. Lawton, B. Münch, J. Rouzade, Destruction of cyanobacterial toxins by semiconductor photocatalysis, Chem. Commun. 1997 (1997) 393– 394.
47. W.F.D. Vilela, A. Minillo, O. Rocha, E.M. Vieira, E.B. Azevedo, Degradation of [D- Leu]-microcystin-LR by solar heterogeneous photocatalysis (TiO2), Solar Energy 86 (2012) 2746–2752.
48. M.G. Antoniou, P.A. Nicolaou, J.A. Shoemaker, A.A. De La Cruz, D.D. Dionysiou, Impact of the morphological properties of thin TiO2 photocatalytic films on the detoxification of water contaminated with the cyanotoxin, microcystin-LR, Appl. Catal., B 91 (2009) 165–173.
49. M.E. Van Apeldoorn, H.P. Van Egmond, G.J.A. Speijers, G.J.I. Bakker, Toxins of cyanobacteria, Mol. Nutr. Food Res. 51 (2007) 7–60.
50. W. Liao, Y. Zhang, M. Zhang, M. Murugananthan, S. Yoshihara, Photoelectrocatalytic degradation of microcystin-LR using Ag/AgCl/TiO2 nanotube arrays electrode under visible light irradiation, Chem. Eng. J. 231 (2013) 455–463.
51. L. Lawton, P. Robertson, B. Cornish, M. Jaspars, Detoxification of

microcystins (cyanobacterial hepatotoxins) using TiO2 photocatalytic oxidation, Environ. Sci. Technol. 33 (1999) 771–775.
52. S. Rudolph-Böhner, D.F. Mierke, L. Moroder, Molecular structure of the cyanobacterial tumor-promoting microcystins, FEBS Lett. 349 (1994) 319–323.
53. A.R. Klein, D.S. Baldwin, E. Silvester, Proton and iron binding by the cyanobacterial toxin microcystin-LR, Environ. Sci. Technol. 47 (2013) 5178–5184.
54. P.G.-J. De Maagd, A.J. Hendriks, W. Seinen, D.T.H.M. Sijm, PH-dependent hydrophobicity of the cyanobacteria toxin microcystin-LR, Water Res. 33 (1999) 677–680.
55. Ohtani, Photocatalysis A to Z – what we know and what we do not know in a scientific sense, J. Photochem. Photobiol. C: Photochem. Rev. 11 (2010) 157– 178.
56. M. Pelaez, A.A. De La Cruz, K. O'shea, P. Falaras, D.D. Dionysiou, Effects of water parameters on the degradation of microcystin-LR under visible light-activated TiO2 photocatalyst, Water Res. 45 (2011) 3787–3796.
57. S.M. Rodríguez, C. Richter, J.B. Gálvez, M. Vincent, Photocatalytic degradation of industrial residual waters, Solar Energy 56 (1996) 401–410.
58. X.G. Feng, F. Rong, T. Wei, C.W. Yuan, Studies of photocatalytic degradation of trace-level MC-LR in water on thin film of titanium dioxide, in: D.A.D.D.P. B (Ed.), China International Conference on Nanoscience and Technology, China NANO 2005, Trans Tech Publications Ltd., Beijing, China, 2005, pp. 951–954.
59. G. Liu, C. Han, M. Pelaez, D. Zhu, S. Liao, V. Likodimos, A.G. Kontos, P. Falaras, D.D. Dionysiou, Enhanced visible light photocatalytic activity of CN-codoped TiO2 films for the degradation of microcystin-LR, J. Mol. Catal. A: Chem. 372 (2013) 58–65.
60. X. He, M. Pelaez, J.A. Westrick, K.E. O'shea, A. Hiskia, T. Triantis, T. Kaloudis, M.I. Stefan, A.A. De La Cruz, D.D. Dionysiou, Efficient removal of microcystin-LR by UV-C/H2O2 in synthetic and natural water samples, Water Res. 46 (2012) 1501–1510.
61. P. Senogles, J. Scott, G. Shaw, H. Stratton, Photocatalytic degradation of the cyanotoxin cylindrospermopsin, using titanium dioxide and UV irradiation, Water Res. 35 (2001) 1245–1255.
62. R.K. Chiswell, G.R. Shaw, G. Eaglesham, M.J. Smith, R.L. Norris, A.A. Seawright, M.R. Moore, Stability of cylindrospermopsin, the toxin from the cyanobacterium, *Cylindrospermopsis raciborskii*: effect of pH, temperature, and sunlight on decomposition, Environ. Toxicol. 14 (1999) 155–161.
63. X. He, A.A. De La Cruz, D.D. Dionysiou, Destruction of cyanobacterial toxin cylindrospermopsin by hydroxyl radicals and sulfate radicals using UV-254 nm activation of hydrogen peroxide, persulfate and peroxymonosulfate, J. Photochem. Photobiol. A: Chem. 251 (2013) 160–166.
64. G.D. Onstad, S. Strauch, J. Meriluoto, G.A. Codd, U. Von Gunten,

Selective oxidation of key functional groups in cyanotoxins during drinking water ozonation, Environ. Sci. Technol. 41 (2007) 4397–4404.
65. Máthé, M. M-Hamvas, G. Vasas, Microcystin-LR and cylindrospermopsin induced alterations in chromatin organization of plant cells, Mar. Drugs 11 (2013) 3689–3717.
66. P.A. Soares, T.F. Silva, D.R. Manenti, S.M. Souza, R.A. Boaventura, V.J. Vilar, Insights into real cotton-textile dyeing wastewater treatment using solar advanced oxidation processes, Environ. Sci. Pollut. Res. 21 (2014) 932–945.

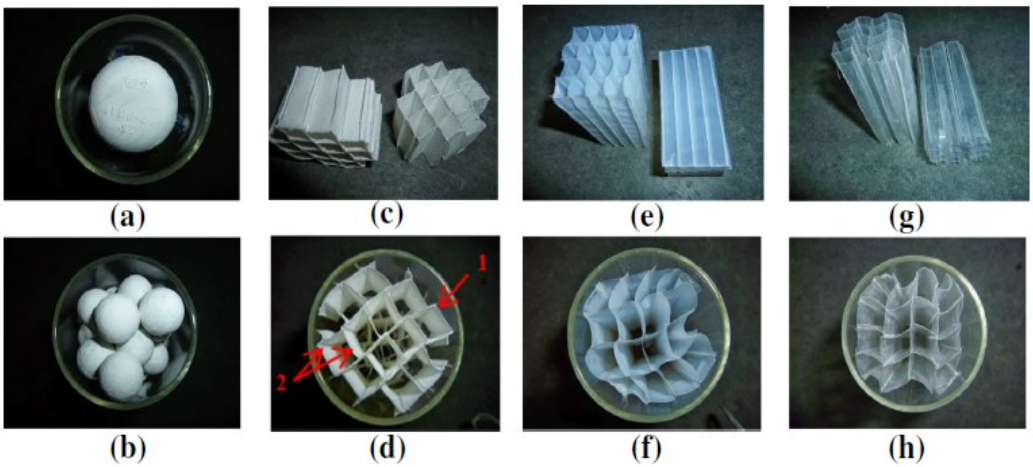

Fig. 1. (a) Catalytic-bed Pnt(4)-PVCT packed into borosilicate tube; (b) catalytic-bed Pnt(4)-GS packed into borosilicate tube; (c) monoliths coated with Pnt(4)-PETM; (d) catalytic-bed Pnt(4)-PETM packed into borosilicate tube, 1: one sheet, 2: two sheets; (e) monoliths coated with P25-CAM; (f) catalytic-bed P25-CAM packed into borosilicate tube; (g) monoliths coated with TiO2-CAM and (h) TiO2-CAM packed into borosilicate tube

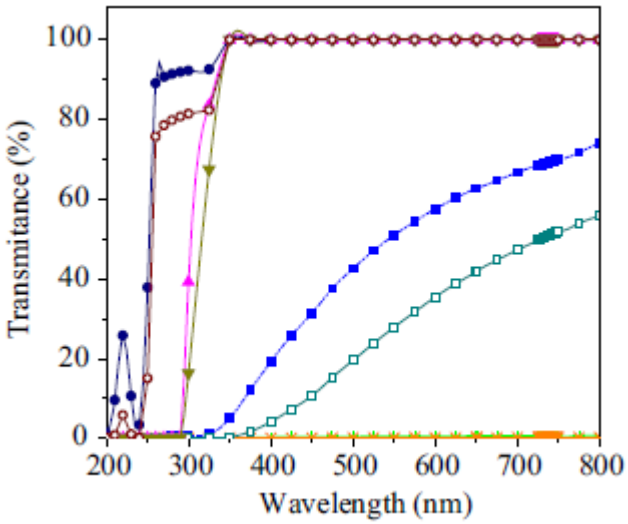

Fig. 2. Normalized absorbance spectra of the material used in the photocatalytic reactions (see the sheets in Fig. 1d): – PETM (1 sheet): without coating; - PETM (2 sheets): without coating; – Pnt(4)-PETM (1 sheet): with TiO_2 coating; – Pnt(4)-PETM (2 sheets): with TiO_2 coating; – CAM (1 sheet): without coating; – CAM (2 sheets): without coating; – P25-CAM (1 sheet): with TiO_2 coating; – P25-CAM (2 sheets): with TiO_2 coating

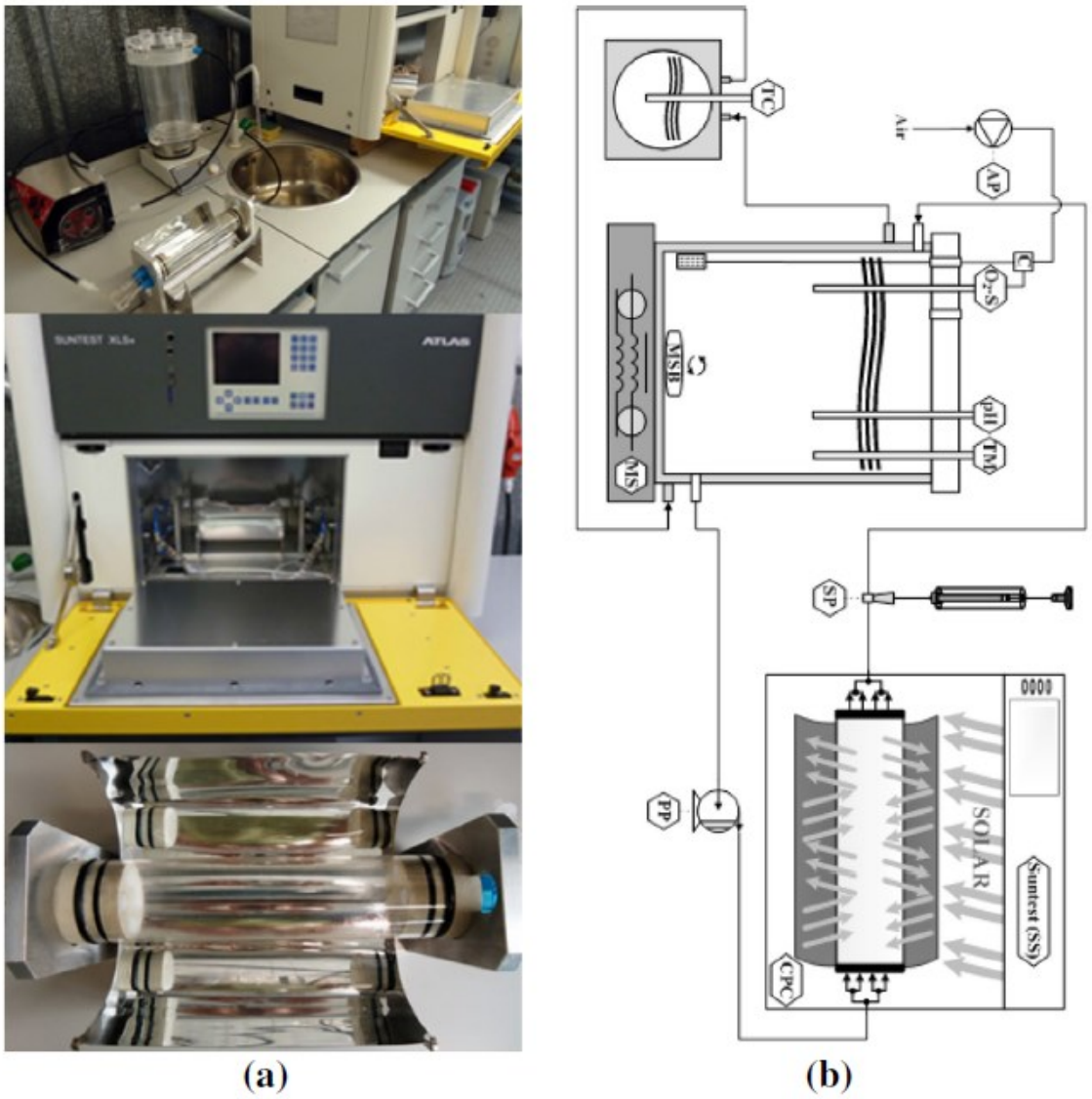

Fig. 3. (a) Photograph and (b) scheme of the lab-scale photocatalytic system: TC – temperature controller; PP – peristaltic pump; AP – air pump; C – controller; O2-S – dissolved oxygen sensor; pH – pH meter; TM – temperature meter; MSB – magnetic bar; MS – magnetic stirrer; CPC – Compound Parabolic Collector; SS – Suntest System; SP – sampling point. Reprinted (adapted) with permission from Soares et al. [66]. Copyright © 2013, Springer-Verlag, Berlin, Heidelberg, License Number: 3190821060851.

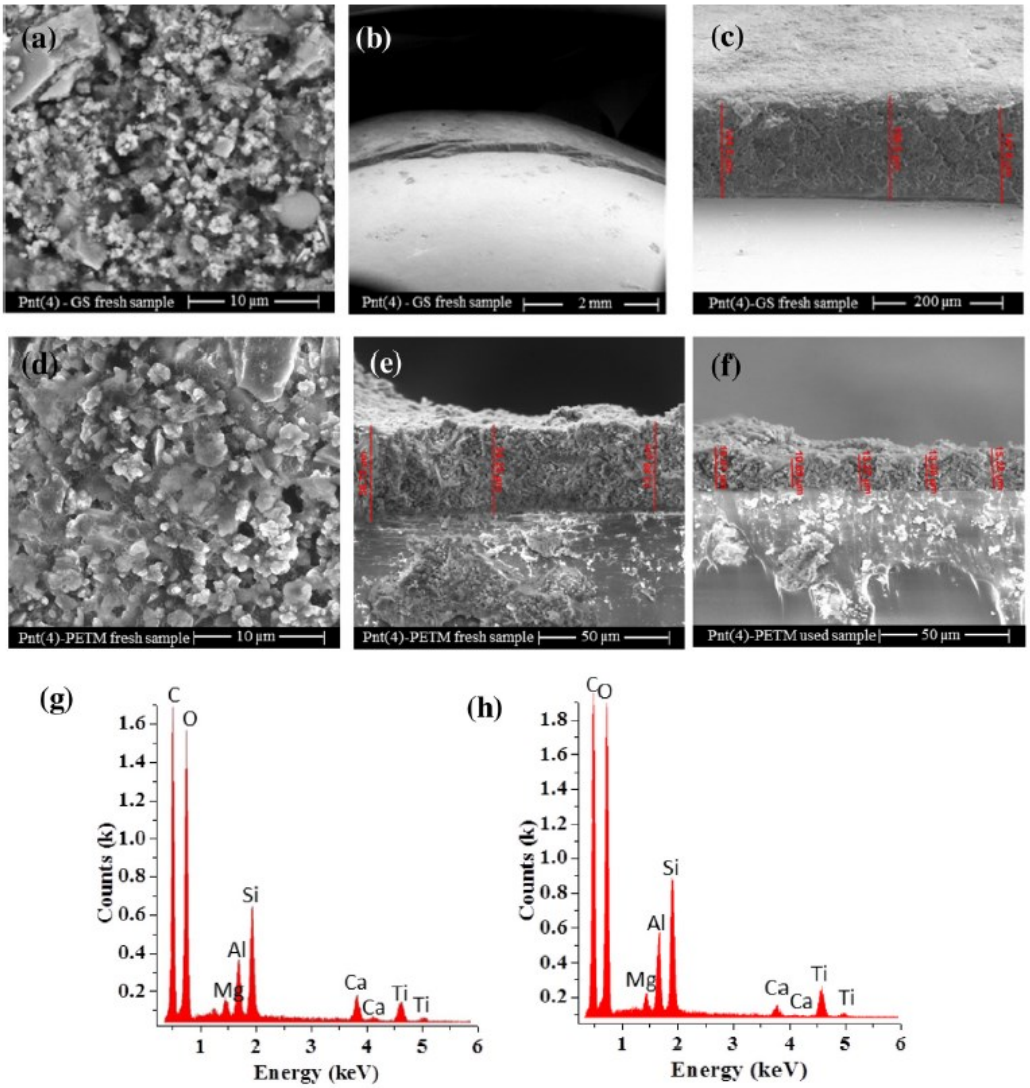

Fig. 4. (a), (b) and (c) SEM micrographs of the fresh sample Pnt(4)-GS; (d), (e) and (f) SEM micrographs of the fresh and used sample Pnt(4)-PETM; (g) and (h) EDX spectra of the sample Pnt(4)-PETM fresh and used respectively.

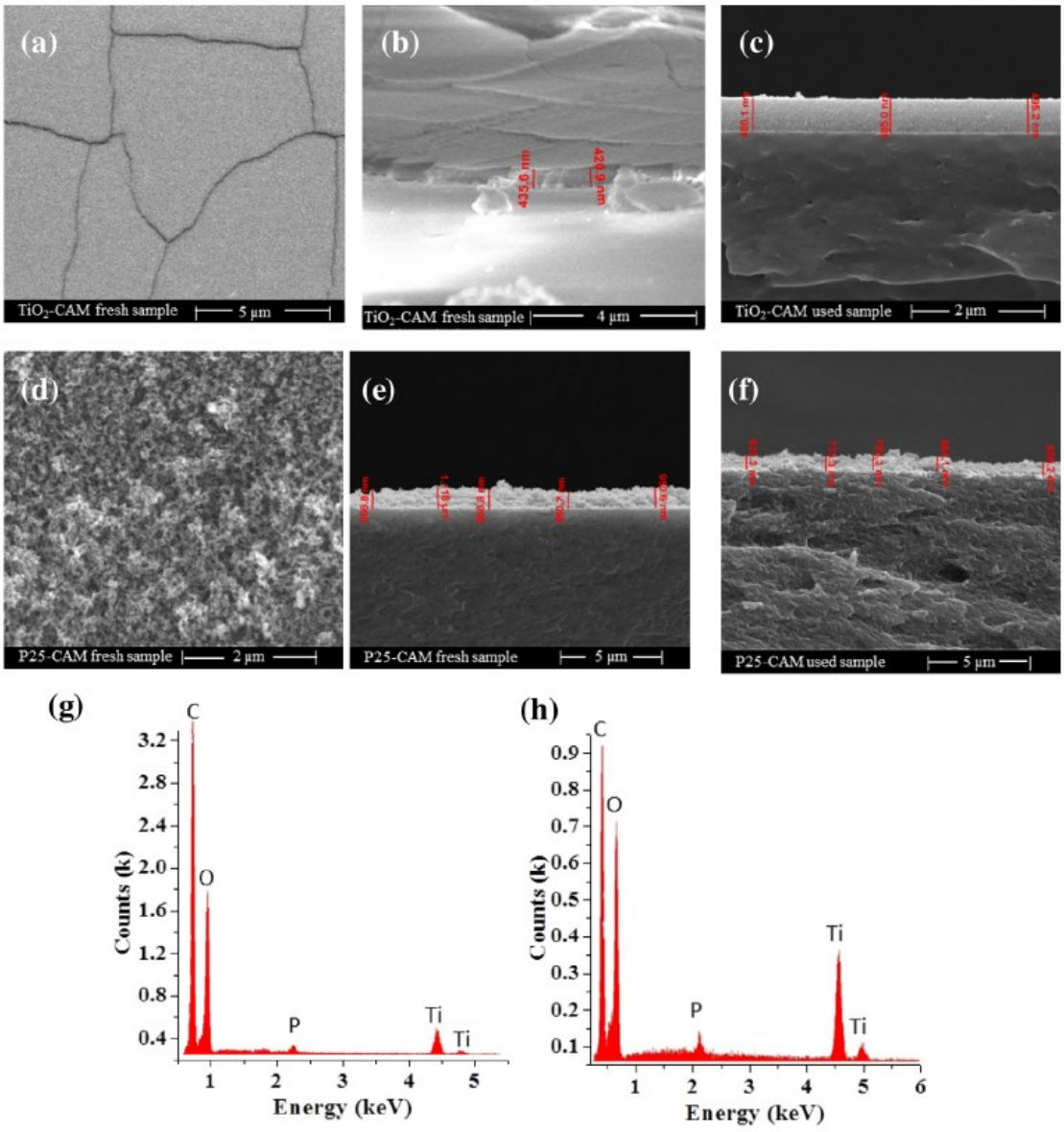

Fig. 5. (a), (b) and (c) SEM micrographs of the fresh and used sample TiO2-CAM; (d), (e) and (f) SEM micrographs of the fresh and used sample P25-CAM; (g) and (h) EDX spectra of TiO2-CAM and P25-CAM respectively, both fresh sample.

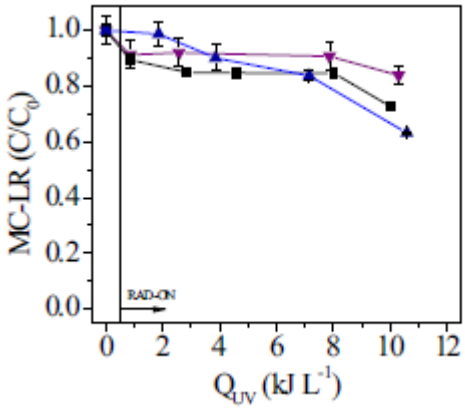

Fig. 6. MC-LR removal by photolysis (simulated solar light) using PVC tube painted with paints without TiO2 addition or H2O2. – Photolysis; – Photolysis with paint; j Photolysis with H2O2

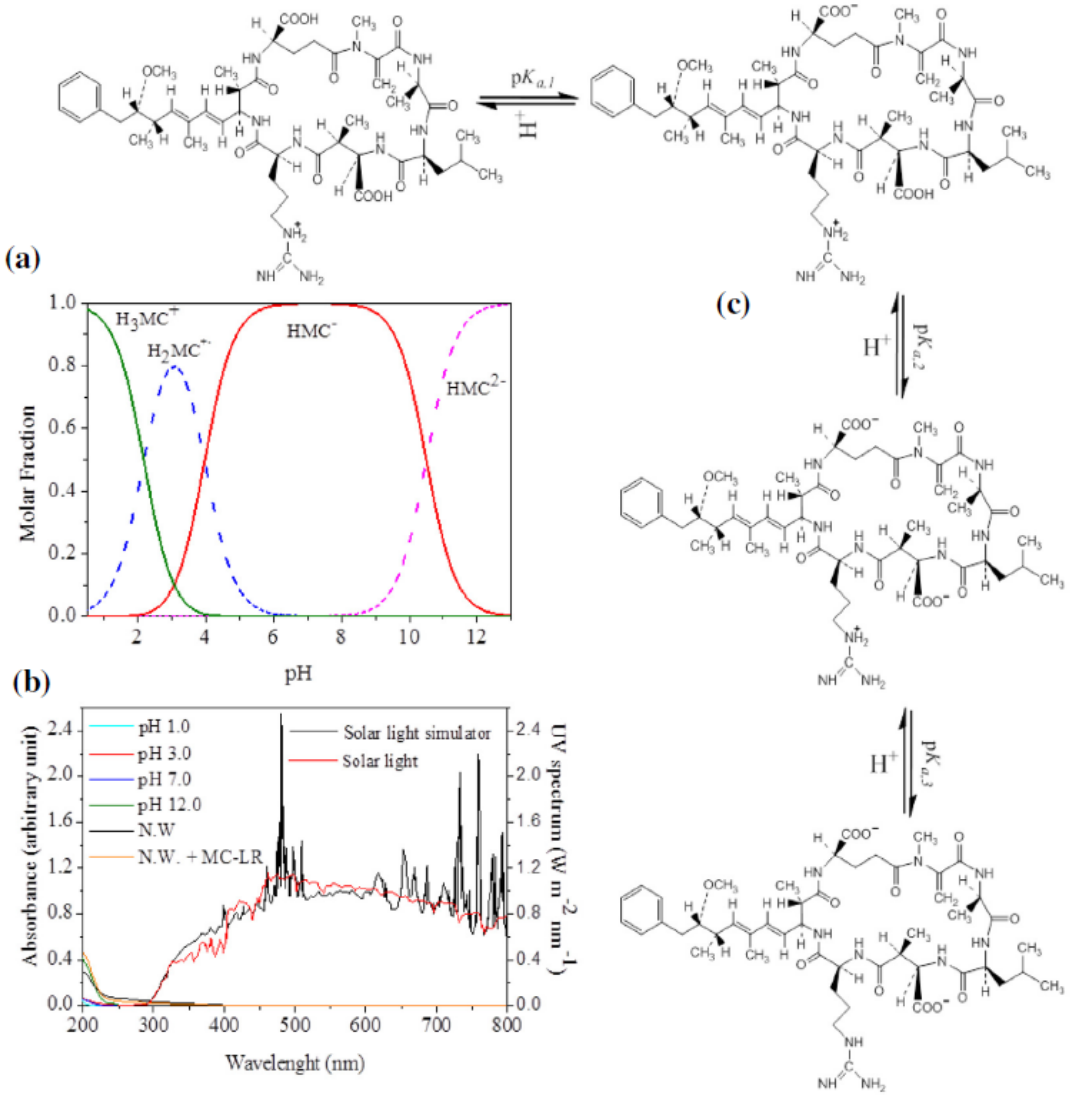

Fig. 7. (a) MC-LR speciation diagram as a function of pH; (b) Normalized absorbance spectra of MC-LR at pH = 1.0, 3.0, 7.0 and 12; of natural water and natural water spiked with MC-LR; simulated and natural solar light spectra; and (c) MC-LR dissociation equilibrium with p*K*a,1 = 2.17 [53], p*K*a,2 = 3.96 [53] and p*K*a,3 = 9.0 [54] (T = 25 ºC, ionic strength = 0 M).

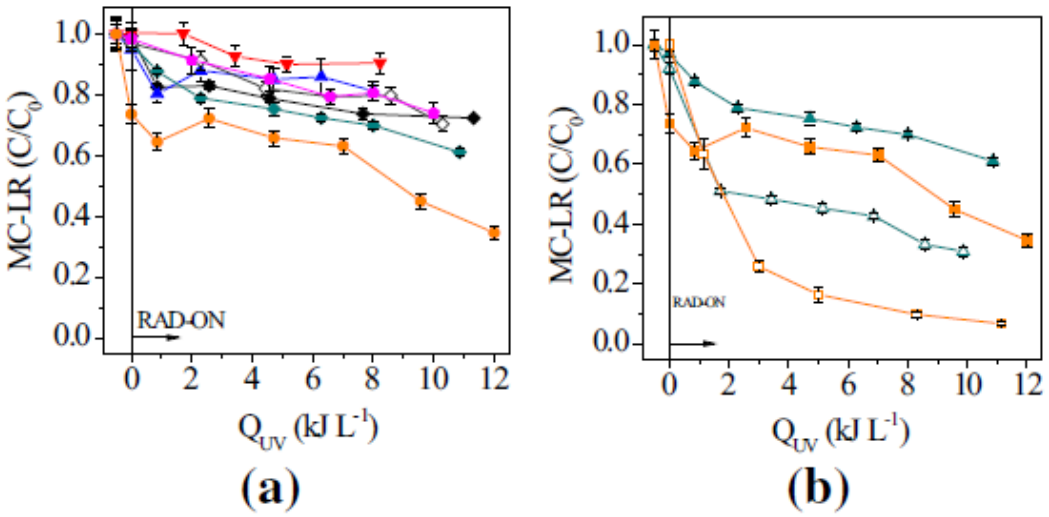

Fig. 8. (a) MC-LR removal by photocatalysis (simulated solar light) using TiO_2-based paints supported in different materials: ♦ – Pnt(1)/UV–vis; ▼ – Pnt(2)/UV–vis; ▲ – Pnt(3)/UV–vis; ◆ – Pnt(4)-PVCT(W)/UV–vis; ◇ – Pnt(4)-PVCT(M)/UV–vis; ⬟ – Pnt(4)-GS/UV–vis; ● – Pnt(4)-PETM/UV–vis; (b) MC-LR removal by photocatalysis (simulated solar light) with and without H_2O_2 using TiO_2-based paint, formulation Pnt(4) supported in PVCT and PETM: ▲ – Pnt(4)-PVCT(W)/UV–vis; △ – Pnt(4)-PVCT(W)/H_2O_2/UV–vis; ■ – Pnt(4)-PETM/UV–vis; □ – Pnt(4)-PETM/H_2O_2/UV–vis.

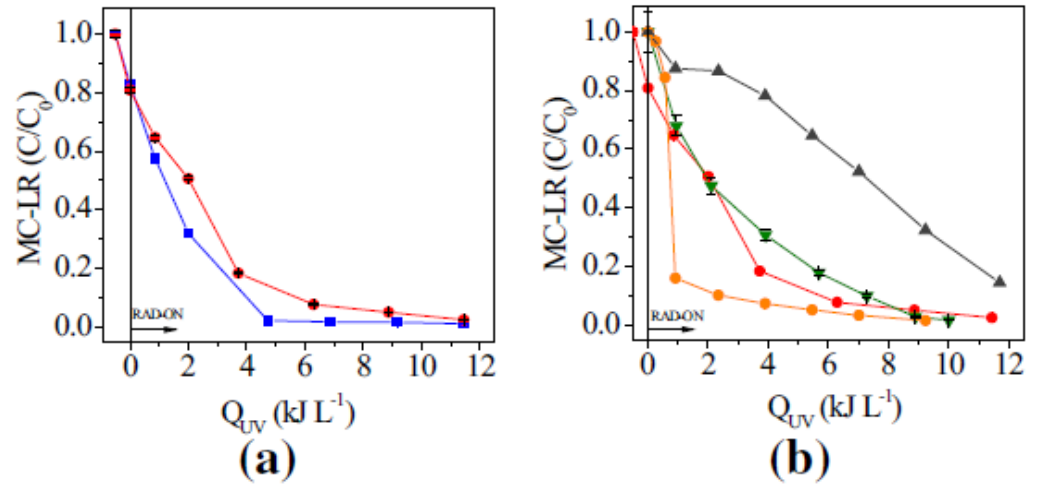

Fig. 9. (a) MC-LR removal by photocatalysis using a catalytic bed with P25-CAM and TiO_2-CAM: ● – P25-CAM/simulated solar light (distilled water); ■ - TiO_2-CAM/simulated solar light (distilled water); (b) MC-LR removal by photocatalysis using P25-CAM, with and without H_2O_2: ● – P25-CAM/simulated solar light (distilled water); ▼ – P25-CAM/natural solar light (distilled water); ● – P25-CAM/H_2O_2/simulated solar light (distilled water); ▲ – P25-CAM/H_2O_2/simulated solar light (river water).

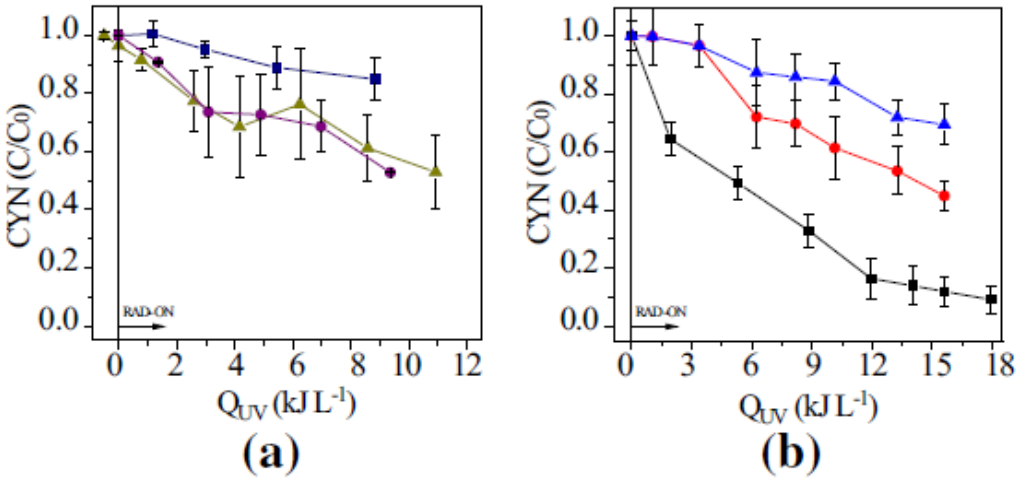

Fig. 10. (a) CYN removal by photolysis and photocatalysis using a P25-CAM catalytic bed: ■ – Photolysis-CYN/simulated solar light (distilled water); ▲ – P25-CAM-CYN/simulated solar light (distilled water); ● – P25-CAM-CYN/natural solar light (distilled water); (b) CYN removal by photocatalysis using P25-CAM/H_2O_2/UV–vis and only H_2O_2/UV–vis: ● – P25-CAM-CYN/H_2O_2/simulated solar light (distilled water); ■ – P25-CAM-CYN/H_2O_2/simulated solar light (river water); ▲ – CYN-H_2O_2/simulated solar light (distilled water).

Table 1
Formulations, characteristics of the TiO2 in the formulations, material used as support and type of MC-LR stock solution.

Catalytic-bed	TiO_2 type	$[TiO_2]$ (%/mg L^{-1})	Pigmentary TiO_2 replacement	Support type	Area (m^2)	MC-LR SS
Pnt(1)	P25	9/75	Half	G. tube	0.013	MeOH:Water*
Pnt(2)	VLP7000	9/75	Half	G. tube	0.013	MeOH:Water*
Pnt(3)	PC500	9/75	Total	G. tube	0.013	MeOH:Water*
Pnt(4)-PVCT(M)	PC500	12/100	Total	PVCT	0.015	MeOH:Water*
Pnt(4)-PVCT(W)	PC500	12/100	Total	PVCT	0.015	Water*
Pnt(4)-PETM	PC500	12/200	Total	PETM	0.10	Water*
Pnt(4)-GS	PC500	12/600	Total	G.S.	0.083	MeOH:Water*
P25-CAM	P25	30 mg L^{-1}	–	CAM	0.10	Water*
TiO_2-CAM	Sol gel	55 mg L^{-1}	–	CAM	0.10	Water*
Photolysis (Pnt)	Photolysis with paint*			PVCT	0.015	MeOH:Water*
Photolysis	Photolysis			–	–	MeOH:Water*

Pnt: Paint; PVCT: PVC tube; PETM: PET Monolith; CAM: Cellulose Acetate Monolith; *without TiO_2; G.: glass; GS: glass spheres; SS: stock solution; MeOH:Water: stock solution in MeOH:water (50:50%); Water: stock solution in water.

Table 2
Water quality parameters of Tâmega river (Torrão reservoir) water.

Parameters	Value
pH	7.3
Temperature	15 °C
Conductivity	43 μS cm^{-1}
Dissolved oxygen	10.2 mg O_2 L^{-1}
Absorbance at 254 nm	0.06
DOC*	2.2 mg C L^{-1}
TDC*	3.7 mg C L^{-1}
DIC*	1.5 mg C L^{-1}
Total dissolved nitrogen	0.8 mg N L^{-1}
Nitrite	0.2 mg NO_2^- L^{-1}
Nitrate	3.0 mg NO_3^- L^{-1}
Sulfate	2.2 mg SO_4^{2-} L^{-1}
Chloride	4.9 mg Cl^- L^{-1}
Phosphate	<0.05 mg PO_4^{3-} L^{-1}
Sodium	4.3 mg Na^+ L^{-1}
Ammonium	0.02 NH_4^+ L^{-1}
Magnesium	0.4 mg Mg^{2+} L^{-1}
Calcium	1.2 mg Ca^{2+} L^{-1}
Dissolved iron	0.5 mg Fe^{2+} L^{-1}

*DOC: Dissolved Organic Carbon; TDC: Total Dissolved Carbon; DIC: Dissolved Inorganic Carbon.

Table 3
Properties of the TiO2 and base paint components [17,23] used in this work for the paints formulation.

TiO_2	Crystal structure	Crystal size (nm)	Surface area $A_{photo\text{-}TiO2}$ ($m^2\ g^{-1}$)		Particle size (μm)	
P25	80% Anatase 20% Rutile	25	50		n.p.	
VLP7000	100% Anatase	~15	>250		n.p.	
PC500	>99% Anatase	5–10	345		1.2–1.7	
Paint components (wt.%)	Pigmentary TiO_2	Water	Extenders ($CaCO_3$ and silicates)	Polymer extender slurry	Binder slurry	Additive* slurry
	18	30	18	8	20	6

n.p.: not provided; *dispersing agents, coalescent, thickeners and others additives.